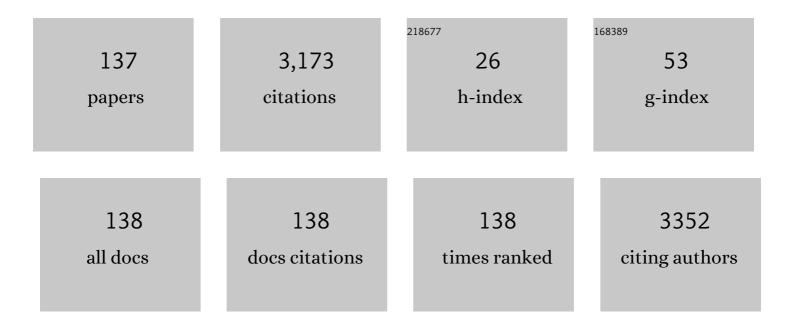
Xavier Briottet

List of Publications by Year in descending order

Source: https://exaly.com/author-pdf/2983829/publications.pdf Version: 2024-02-01



YAVIED RDIOTTET

#	Article	IF	CITATIONS
1	Hyperspectral Pansharpening: A Review. IEEE Geoscience and Remote Sensing Magazine, 2015, 3, 27-46.	9.6	593
2	Selection and characterization of Saharan and Arabian desert sites for the calibration of optical satellite sensors. Remote Sensing of Environment, 1996, 58, 101-114.	11.0	269
3	Shadow detection in very high spatial resolution aerial images: A comparative study. ISPRS Journal of Photogrammetry and Remote Sensing, 2013, 80, 21-38.	11.1	159
4	Adapting cities to climate change: A systemic modelling approach. Urban Climate, 2014, 10, 407-429.	5.7	154
5	Solar panels reduce both global warming and urban heat island. Frontiers in Environmental Science, 2014, 2, .	3.3	137
6	Results of POLDER in-flight calibration. IEEE Transactions on Geoscience and Remote Sensing, 1999, 37, 1550-1566.	6.3	127
7	The Canopy and Aerosol Particles Interactions in TOulouse Urban Layer (CAPITOUL) experiment. Meteorology and Atmospheric Physics, 2008, 102, 135-157.	2.0	124
8	Linear–Quadratic Mixing Model for Reflectances in Urban Environments. IEEE Transactions on Geoscience and Remote Sensing, 2014, 52, 544-558.	6.3	101
9	Estimation of Soil Moisture Content from the Spectral Reflectance of Bare Soils in the 0.4–2.5 µm Domain. Sensors, 2015, 15, 3262-3281.	3.8	90
10	Influence of Water Content on Spectral Reflectance of Leaves in the 3–15- \$muhbox{m}\$ Domain. IEEE Geoscience and Remote Sensing Letters, 2011, 8, 143-147.	3.1	78
11	Linear-Quadratic Blind Source Separation Using NMF to Unmix Urban Hyperspectral Images. IEEE Transactions on Signal Processing, 2014, 62, 1822-1833.	5.3	75
12	Direct and inverse radiative transfer solutions for visible and near-infrared hyperspectral imagery. IEEE Transactions on Geoscience and Remote Sensing, 2005, 43, 1552-1562.	6.3	68
13	MARMIT: A multilayer radiative transfer model of soil reflectance to estimate surface soil moisture content in the solar domain (400–2500â€~nm). Remote Sensing of Environment, 2018, 217, 1-17.	11.0	64
14	Sensitivity of clay content prediction to spectral configuration of VNIR/SWIR imaging data, from multispectral to hyperspectral scenarios. Remote Sensing of Environment, 2018, 204, 18-30.	11.0	61
15	Evaluating the sensitivity of clay content prediction to atmospheric effects and degradation of image spatial resolution using Hyperspectral VNIR/SWIR imagery. Remote Sensing of Environment, 2015, 164, 1-15.	11.0	57
16	The MISTIGRI thermal infrared project: scientific objectives and mission specifications. International Journal of Remote Sensing, 2013, 34, 3437-3466.	2.9	52
17	Influence of soil moisture content on spectral reflectance of bare soils in the 0.4–14 μm domain. International Journal of Remote Sensing, 2013, 34, 2268-2285.	2.9	44
18	Reassessment of the temperature-emissivity separation from multispectral thermal infrared data: Introducing the impact of vegetation canopy by simulating the cavity effect with the SAIL-Thermique model. Remote Sensing of Environment, 2017, 198, 160-172.	11.0	34

#	Article	IF	CITATIONS
19	Traceable radiometry underpinning terrestrial- and helio-studies (TRUTHS). Advances in Space Research, 2003, 32, 2253-2261.	2.6	33
20	Partial Linear NMF-Based Unmixing Methods for Detection and Area Estimation of Photovoltaic Panels in Urban Hyperspectral Remote Sensing Data. Remote Sensing, 2019, 11, 2164.	4.0	32
21	Criteria Comparison for Classifying Peatland Vegetation Types Using In Situ Hyperspectral Measurements. Remote Sensing, 2017, 9, 748.	4.0	31
22	Monitoring land surface processes with thermal infrared data: Calibration of SVAT parameters based on the optimisation of diurnal surface temperature cycling features. Remote Sensing of Environment, 2008, 112, 872-887.	11.0	29
23	ICARE: A physically-based model to correct atmospheric and geometric effects from high spatial and spectral remote sensing images over 3D urban areas. Meteorology and Atmospheric Physics, 2008, 102, 209-222.	2.0	29
24	Improvement of Soil Moisture Retrieval from Hyperspectral VNIR-SWIR Data Using Clay Content Information: From Laboratory to Field Experiments. Remote Sensing, 2015, 7, 3184-3205.	4.0	29
25	Revisiting Pseudo Invariant Calibration Sites (PICS) Over Sand Deserts for Vicarious Calibration of Optical Imagers at 20 km and 100 km Scales. Remote Sensing, 2019, 11, 1166.	4.0	28
26	A Physics-Based Unmixing Method to Estimate Subpixel Temperatures on Mixed Pixels. IEEE Transactions on Geoscience and Remote Sensing, 2015, 53, 1894-1906.	6.3	27
27	Inertia-Constrained Pixel-by-Pixel Nonnegative Matrix Factorisation: A Hyperspectral Unmixing Method Dealing with Intra-Class Variability. Remote Sensing, 2018, 10, 1706.	4.0	27
28	Monte Carlo approach for solving the radiative transfer equation over mountainous and heterogeneous areas. Applied Optics, 1999, 38, 7419.	2.1	26
29	Thermal infrared radiance simulation with aggregation modeling (TITAN): an infrared radiative transfer model for heterogeneous three-dimensional surfaceapplication over urban areas. Applied Optics, 2008, 47, 5799.	2.1	24
30	Monitoring LAI, Chlorophylls, and Carotenoids Content of a Woodland Savanna Using Hyperspectral Imagery and 3D Radiative Transfer Modeling. Remote Sensing, 2020, 12, 28.	4.0	24
31	Radiative transfer solution for rugged and heterogeneous scene observations. Applied Optics, 2000, 39, 6830.	2.1	23
32	Detection of individual trees in urban alignment from airborne data and contextual information: A marked point process approach. ISPRS Journal of Photogrammetry and Remote Sensing, 2018, 146, 197-210.	11.1	20
33	Phenological Dynamics Characterization of Alignment Trees with Sentinel-2 Imagery: A Vegetation Indices Time Series Reconstruction Methodology Adapted to Urban Areas. Remote Sensing, 2020, 12, 639.	4.0	20
34	North Africa and Saudi Arabia Day/Night Sandstorm Survey (NASCube). Remote Sensing, 2017, 9, 896.	4.0	17
35	Analysis of the Performance of the TES Algorithm Over Urban Areas. IEEE Transactions on Geoscience and Remote Sensing, 2014, 52, 6989-6998.	6.3	16
36	Calibration of SPOT4 HRVIR and Vegetation cameras over Rayleigh scattering. , 2000, 4135, 302.		15

#	Article	IF	CITATIONS
37	Simulation Study of View Angle Effects on Thermal Infrared Measurements Over Heterogeneous Surfaces. IEEE Transactions on Geoscience and Remote Sensing, 2004, 42, 664-672.	6.3	15
38	Retrieval of microphysical and optical properties in aerosol plumes with hyperspectral imagery: L-APOM method. Remote Sensing of Environment, 2009, 113, 781-793.	11.0	15
39	<title>Presentation of a new BRDF measurement device</title> ., 1998, , .		14
40	Assimilation method to derive spectral ground reflectance of desert sites from satellite datasets. Remote Sensing of Environment, 2003, 87, 359-370.	11.0	14
41	<title>Comparison of measured and modeled BRDF of natural targets</title> . , 1999, , .		13
42	Remote sensing of aerosol plumes: a semianalytical model. Applied Optics, 2008, 47, 1851.	2.1	12
43	AMARTIS ν2: 3D Radiative Transfer Code in the [0.4; 2.5 Âμm] Spectral Domain Dedicated to Urban Areas. Remote Sensing, 2011, 3, 1914-1942.	4.0	12
44	Multi-Resolution Study of Thermal Unmixing Techniques over Madrid Urban Area: Case Study of TRISHNA Mission. Remote Sensing, 2019, 11, 1251.	4.0	12
45	Object-based fusion for urban tree species classification from hyperspectral, panchromatic and nDSM data. International Journal of Remote Sensing, 2019, 40, 5339-5365.	2.9	12
46	Joint Use of PROSAIL and DART for Fast LUT Building: Application to Gap Fraction and Leaf Biochemistry Estimations over Sparse Oak Stands. Remote Sensing, 2020, 12, 2925.	4.0	11
47	HYPXIM: A new hyperspectral sensor combining science/defence applications. , 2011, , .		10
48	Simultaneous retrieval of CO ₂ and aerosols in a plume from hyperspectral imagery: application to the characterization of forest fire smoke using AVIRIS data. International Journal of Remote Sensing, 2013, 34, 6837-6864.	2.9	10
49	A repeatable change detection approach to map extreme storm-related damages caused by intense surface runoff based on optical and SAR remote sensing: Evidence from three case studies in the South of France. ISPRS Journal of Photogrammetry and Remote Sensing, 2021, 182, 153-175.	11.1	10
50	Aggregation process of optical properties and temperature over heterogeneous surfaces in infrared domain. Applied Optics, 2010, 49, 4655.	2.1	9
51	Montmorillonite Estimation in Clay–Quartz–Calcite Samples from Laboratory SWIR Imaging Spectroscopy: A Comparative Study of Spectral Preprocessings and Unmixing Methods. Remote Sensing, 2020, 12, 1723.	4.0	9
52	Impact of contextual information integration on pixel fusion. IEEE Transactions on Geoscience and Remote Sensing, 2002, 40, 1997-2010.	6.3	8
53	Efficient Empirical Reflectance Retrieval in Urban Environments. IEEE Journal of Selected Topics in Applied Earth Observations and Remote Sensing, 2013, 6, 1596-1601.	4.9	8
54	Detection And Area Estimation For Photovoltaic Panels In Urban Hyperspectral Remote Sensing Data By		8

An Original Nmf-Based Unmixing Method. , 2018, , .

#	Article	IF	CITATIONS
55	Night Thermal Unmixing for the Study of Microscale Surface Urban Heat Islands with TRISHNA-Like Data. Remote Sensing, 2019, 11, 1449.	4.0	8
56	Intercalibration of optical satellites $\hat{a} \in $ a case study with MOMS and SPOT. Aerospace Science and Technology, 2001, 5, 305-315.	4.8	7
57	Phenomenological Analysis of Simulated Signals Observed Over Shaded Areas in an Urban Scene. IEEE Transactions on Geoscience and Remote Sensing, 2004, 42, 434-442.	6.3	7
58	Sensor radiance physical model for rugged heterogeneous surfaces in the 3-14 μm region Optics Express, 2006, 14, 2130.	3.4	7
59	A nonlinear unmixing method in the infrared domain. Applied Optics, 2011, 50, 3666.	2.1	7
60	Remote sensing of aerosols in urban areas from very high spatial resolution images: application of the OSIS code to multispectral PELICAN airborne data. International Journal of Remote Sensing, 2013, 34, 919-937.	2.9	7
61	HYPXIM: A second generation high spatial resolution hyperspectral satellite for dual applications. , 2013, , .		7
62	Comparison of two atmospheric correction methods for the classification of spaceborne urban hyperspectral data depending on the spatial resolution. International Journal of Remote Sensing, 2018, 39, 1593-1614.	2.9	7
63	Anthropogenic aerosol emissions mapping and characterization by imaging spectroscopy – application to a metallurgical industry and a petrochemical complex. International Journal of Remote Sensing, 2019, 40, 364-406.	2.9	7
64	Analysis and quantification of seabed adjacency effects in the subsurface upward radiance in shallow waters. Optics Express, 2019, 27, A319.	3.4	7
65	A random forest class memberships based wrapper band selection criterion: Application to hyperspectral. , 2015, , .		6
66	Mapping Benthic Habitats by Extending Non-Negative Matrix Factorization to Address the Water Column and Seabed Adjacency Effects. Remote Sensing, 2020, 12, 2072.	4.0	6
67	Impact of the number of dates and their sampling on a NDVI time series reconstruction methodology to monitor urban trees with Ven14s satellite. International Journal of Applied Earth Observation and Geoinformation, 2021, 95, 102257.	2.8	6
68	Traceable radiometry underpinning terrestrial- and helio-studies (TRUTHS). , 2003, , .		5
69	Hyperspectral reconnaissance in urban environment. , 2013, , .		5
70	Simulating Space Lidar Waveforms From Smaller-Footprint Airborne Laser Scanner Data for Vegetation Observation. IEEE Geoscience and Remote Sensing Letters, 2014, 11, 534-538.	3.1	5
71	ICARE-VEG: A 3D physics-based atmospheric correction method for tree shadows in urban areas. ISPRS Journal of Photogrammetry and Remote Sensing, 2018, 142, 311-327.	11.1	5
72	Potentiel de l'imagerie optique satellitaire à haute résolution pour détecter les dommages engendrés par des épisodes pluvieux extrêmes. Houille Blanche, 2020, 106, 66-74.	0.3	5

#	Article	IF	CITATIONS
73	Aerosols in urban areas: optical properties and impact on the signal incident to an airborne high-spatial resolution camera. , 2008, , .		4
74	Soil moisture impact on lab measured reflectance of bare soils in the optical domain [0.4–15 μM]. , 2009, , .		4
75	A linear-quadratic unsupervised hyperspectral unmixing method dealing with intra-class variability. , 2016, , .		4
76	Classification of peatland vegetation types using in situ hyperspectral measurements. , 2017, , .		4
77	Individual Tree Crown Delineation Method Based on Multi-Criteria Graph Using Geometric and Spectral Information: Application to Several Temperate Forest Sites. Remote Sensing, 2022, 14, 1083.	4.0	4
78	Hyperspectral Pansharpening in the Reflective Domain with a Second Panchromatic Channel in the SWIR II Spectral Domain. Remote Sensing, 2022, 14, 113.	4.0	4
79	Characterization of desert areas with Meteosat-4 data for the calibration of optical satellite sensors. , 1993, , .		3
80	<title>POLDER multiangular calibration using desert sites: method and performances</title> . , 1997, 3221, 141.		3
81	SPOT calibration of blue and green channels using Rayleigh scattering over clear oceans. , 1997, , .		3
82	<title>Vegetation calibration of blue and red channels using Rayleigh scattering over open oceans</title> . , 1997, , .		3
83	Detection in urban scenario using combined airborne imaging sensors. Proceedings of SPIE, 2012, , .	0.8	3
84	Use intermediate results of wrapper band selection methods: A first step toward the optimization of spectral configuration for land cover classifications. , 2014, , .		3
85	An unmixing-based method for the analysis of thermal hyperspectral images. , 2014, , .		3
86	Identify important spectrum bands for classification using importances of wrapper selection applied to hyperspectral data. , 2014, , .		3
87	Radiometry in the Optical Domain. , 2016, , 1-56.		3
88	A sub km resolution global database of surface reflectance and emissivity based on 10-years of MODIS data. ISPRS Journal of Photogrammetry and Remote Sensing, 2016, 122, 222-235.	11.1	3
89	Application and Extension of PCA Concepts to Blind Unmixing of Hyperspectral Data with Intra-class Variability. , 2018, , 225-252.		3
90	Using a Panchromatic Image to Improve Hyperspectral Unmixing. Remote Sensing, 2020, 12, 2834.	4.0	3

#	Article	IF	CITATIONS
91	Spectral Unmixing for Thermal Infrared Multi-Spectral Airborne Imagery over Urban Environments: Day and Night Synergy. Remote Sensing, 2020, 12, 1871.	4.0	3
92	A Simulation-Based Error Budget of the TES Method for the Design of the Spectral Configuration of the Micro-Bolometer-Based MISTIGRI Thermal Infrared Sensor. IEEE Transactions on Geoscience and Remote Sensing, 2022, 60, 1-19.	6.3	3
93	Impact of Tree Crown Transmittance on Surface Reflectance Retrieval in the Shade for High Spatial Resolution Imaging Spectroscopy: A Simulation Analysis Based on Tree Modeling Scenarios. Remote Sensing, 2021, 13, 931.	4.0	3
94	Impact of Modeling Abstractions When Estimating Leaf Mass per Area and Equivalent Water Thickness over Sparse Forests Using a Hybrid Method. Remote Sensing, 2021, 13, 3235.	4.0	3
95	<title>SPOT4: first in-flight absolute calibration results</title> . , 1998, , .		2
96	Directional effect on change of spatial scale over heterogeneous surface in thermal infrared remote sensing. , 2002, , .		2
97	Remote sensing of aerosols in urban areas: sun/shadow retrieval procedure from airborne very high spatial resolution images. , 2009, , .		2
98	OSIS: remote sensing code for estimating aerosol optical properties in urban areas from very high spatial resolution images. Applied Optics, 2011, 50, 5408.	2.1	2
99	Physic based aggregation model for the unmixing of temperature and optical properties in the infrared domain. , 2012, , .		2
100	Performance analysis of unsupervised unmixing models for thermal hyepsrpectral. , 2012, , .		2
101	Material reflectance retrieval in urban tree shadows with physics-based empirical atmospheric correction. , 2013, , .		2
102	A method based on nonnegative matrix factorization dealing with intra-class variability for unsupervised hyperspectral unmixing. , 2015, , .		2
103	Development and validation of a numerical tool for simulating the surface temperature field and the infrared radiance rendering in an urban scene. Quantitative InfraRed Thermography Journal, 2015, 12, 196-218.	4.2	2
104	Background Radiance Estimation for Gas Plume Quantification for Airborne Hyperspectral Thermal Imaging. Journal of Spectroscopy, 2016, 2016, 1-17.	1.3	2
105	Optical Remote Sensing in Urban Environments. , 2016, , 1-62.		2
106	Hierarchically exploring the width of spectral bands for urban material classification. , 2017, , .		2
107	A New Hyperspectral Unmixing Method Using Co-Registered Hyperspectral and Panchromatic Images. , 2019, , .		2
108	Validation of an empirical method for thin cirrus correction with Sentinel-2 data. , 2019, , .		2

#	Article	IF	CITATIONS
109	Construction of a Global Database of Surface Reflectance and Emissivity at a Sub km Resolution. Progress in Electromagnetics Research Symposium: [proceedings] Progress in Electromagnetics Research Symposium, 2010, 6, 195-200.	0.4	2
110	Proxy Data of Surface Water Floods in Rural Areas: Application to the Evaluation of the IRIP Intense Runoff Mapping Method Based on Satellite Remote Sensing and Rainfall Radar. Water (Switzerland), 2022, 14, 393.	2.7	2
111	A New Material-Oriented TES for Land Surface Temperature and SUHI Retrieval in Urban Areas: Case Study over Madrid in the Framework of the Future TRISHNA Mission. Remote Sensing, 2021, 13, 5139.	4.0	2
112	<title>Evaluation of the different irradiance components on a rugged terrain</title> . , 1998, 3494, 41.		1
113	Hyperspectral remote sensing of biomass burning aerosol plumes: sensitivity to optical properties modeling. , 2006, , .		1
114	Radiative modeling and characterization of aerosol plumes in hyperspectral imagery. , 2007, , .		1
115	TITAN: a new infrared radiative transfer model for the study of heterogeneous 3D surface. Proceedings of SPIE, 2008, , .	0.8	1
116	A physics-based unmixing method for thermal hyperspectral images. , 2014, , .		1
117	A non-linear optimal estimator for plume concentration retrieval, using airborne hyperspectral measurement. , 2014, , .		1
118	Characterization of hyperspectral images prior to unmixing, based on eigendecompositions and sum-to-one condition. , 2014, , .		1
119	Hyperspectral pansharpening based on unmixing techniques. , 2015, , .		1
120	Performance assessment of simulated 3D laser images using Geiger-mode avalanche photo-diode: tests on simple synthetic scenarios. Proceedings of SPIE, 2015, , .	0.8	1
121	Corrigendum to "Background Radiance Estimation for Gas Plume Quantification for Airborne Hyperspectral Thermal Imaging― Journal of Spectroscopy, 2016, 2016, 1-4.	1.3	1
122	ICARE-HS: atmospheric correction of airborne hyperspectral urban images using 3D information. Proceedings of SPIE, 2016, , .	0.8	1
123	Using 3D information for atmospheric correction of airborne hyperspectral images of urban areas. , 2017, , .		1
124	Land Surface Temperature Retrieval over Urban areas from simulated TRISHNA data. , 2019, , .		1
125	Applications in remote sensing—anthropogenic activities. Data Handling in Science and Technology, 2020, 32, 411-452.	3.1	1
126	<title>On-board calibration device for a wide field-of-view instrument</title> . , 1991, , .		0

#	Article	IF	CITATIONS
127	Combined field [3 to 5 μ m] and [8 to 14 μ m] infrared imaging: approaches to extracting target's bidirectional reflectivity and emissivity. , 2002, 4538, 1.		Ο
128	Modelling of aggregation and disaggregation of optical properties and surface temperatures over urban area in infrared domain. , 2009, , .		0
129	The comparability of aggregated emissivity and temperature of heterogeneous pixel to conventional tes methods. , 2013, , .		Ο
130	SYSIPHE, airborne hyperspectral system: Focus on the SIELETERS thermal hyperspectral imaging instrument. , 2013, , .		0
131	Mosa $ ilde{A}$ c active imaging: direct physical modeling and image reconstruction. Proceedings of SPIE, 2014, , .	0.8	0
132	A comparison of several feature selection scores applied to hyperspectral data. , 2015, , .		0
133	Characterization of Industrial Plumes. , 2016, , 97-146.		Ο
134	Comparison of simulated and experimental 3D laser images using a GmAPD array: application to long range detection. Proceedings of SPIE, 2016, , .	0.8	0
135	Identification of the London plane in urban alignment based on hyperspectral data and contextual information. , 2019, , .		0
136	Relations Between Landsat Spectral Reflectances and Land Surface Emissivity Over Bare Soils. , 2019, , .		0
137	Spectral Optimization of Airborne Multispectral Camera for Land Cover Classification: Automatic Feature Selection and Spectral Band Clustering. , 0, , .		Ο